

# A Potent D-Protein Antagonist of VEGF-A is Nonimmunogenic, Metabolically Stable, and Longer-Circulating *in Vivo*

Maruti Uppalapati,<sup>†,∇,◆</sup> Dong Jun Lee,<sup>‡,○,◆</sup> Kalyaneswar Mandal,<sup>‡</sup> Hongyan Li,<sup>§</sup> Les P. Miranda,<sup>||</sup> Joshua Lowitz,<sup>⊥</sup> John Kenney,<sup>⊥</sup> Jarrett J. Adams,<sup>†</sup> Dana Ault-Riché,<sup>#</sup> Stephen B. H. Kent,<sup>\*,‡</sup> and Sachdev S. Sidhu<sup>\*,†</sup>

<sup>†</sup>Banting and Best Department of Medical Research and Department of Molecular Genetics, the Donnelly Centre, University of Toronto, Toronto, Ontario, Canada M5S 3E1

<sup>‡</sup>Department of Chemistry; Department of Biochemistry and Molecular Biology, Institute for Biophysical Dynamics, University of Chicago, Chicago, Illinois 60637, United States

<sup>§</sup>Pharmacokinetics & Drug Metabolism, Amgen, Inc., Thousand Oaks, California 91320, United States

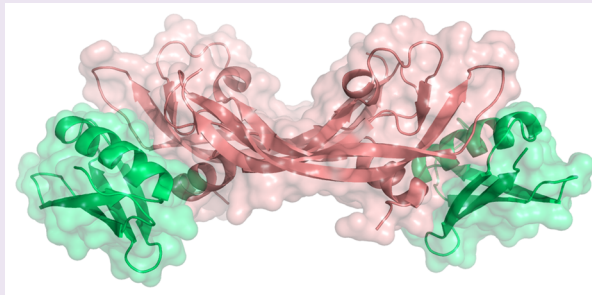
<sup>||</sup>Therapeutic Discovery, Amgen, Inc., Thousand Oaks, California 91320, United States

<sup>⊥</sup>Antibody Solutions, Sunnyvale, California 94089, United States

<sup>#</sup>Reflexion Pharmaceuticals, Inc., San Francisco, California 94104, United States

## Supporting Information

**ABSTRACT:** Polypeptides composed entirely of D-amino acids and the achiral amino acid glycine (D-proteins) inherently have *in vivo* properties that are proposed to be near-optimal for a large molecule therapeutic agent. Specifically, D-proteins are resistant to degradation by proteases and are anticipated to be non-immunogenic. Furthermore, D-proteins are manufactured chemically and can be engineered to have other desirable properties, such as improved stability, affinity, and pharmacokinetics. Thus, a well-designed D-protein therapeutic would likely have significant advantages over L-protein drugs. Toward the goal of developing D-protein therapeutics, we previously generated RFX001.D, a D-protein antagonist of natural vascular endothelial growth factor A (VEGF-A) that inhibited binding to its receptor. However, RFX001.D is unstable at physiological temperatures ( $T_m = 33$  °C). Here, we describe RFX037.D, a variant of RFX001.D with extreme thermal stability ( $T_m > 95$  °C), high affinity for VEGF-A ( $K_d = 6$  nM), and improved receptor blocking. Comparison of the two enantiomeric forms of RFX037 revealed that the D-protein is more stable in mouse, monkey, and human plasma and has a longer half-life *in vivo* in mice. Significantly, RFX037.D was nonimmunogenic in mice, whereas the L-enantiomer generated a strong immune response. These results confirm the potential utility of synthetic D-proteins as alternatives to therapeutic antibodies.



Monoclonal antibodies, molecules with intrinsic high specificities and affinities for their targets, have been adopted for clinical use as human therapeutics with great success. However, major drawbacks to this technology are immunogenicity and the limitations imposed by the large size and structural complexity of antibodies, which can impede the generation of new or improved molecules.<sup>1</sup> Consequently, there is great interest in developing new strategies to efficiently create molecules that bind medically relevant targets with high affinity and specificity, and which can also obviate such issues.<sup>2,3</sup> Several novel scaffolds have been developed to engineer proteins, but these have limited appeal for producing therapeutics as their products are often immunogenic and have short half-lives due to renal clearance and proteolytic degradation.<sup>3</sup>

An underexplored but highly promising alternative approach is to engineer chemically synthesized D-proteins, comprised

entirely of D-amino acids and the achiral amino acid glycine, to bind and modify the behavior of natural L-proteins. A D-amino acid is the enantiomer of an L-amino acid, and for a given sequence, the resulting D- and L-proteins have mirror image structures. It has long been recognized that natural L-protein receptors, enzymes, and especially proteases will not bind the mirror image D-protein form of their natural targets.<sup>4</sup> This would permit the D-protein to resist proteolytic degradation and avoid triggering an immune response, and indeed, this has been observed in the case of rubredoxin.<sup>5</sup> Resistance to proteolytic degradation, and the lack of immunogenicity, are likely intrinsic properties of D-proteins. Furthermore, D-proteins

Received: December 7, 2015

Accepted: January 8, 2016

Table 1. Synthetic D-Proteins

protein	sequence	$T_m^a$	$K_d^b$
RFX001.D	tyklilnGktlkGettveavdvdafdvffvyaasnsfdddwtyddatktftvte	33	85
RFX035.D	mkieehhhhhhhhhGGstykilnGktlkGettveavdvdafdvffvyaasnsfdddwtyddatktftvteGGsdk	82	
RFX037.D	rrrrrGGstykilnGktlkGettveavdvdafdvffvyaasnsfdddwtyddatktftvteGGsdk	93	6

<sup>a</sup>Thermal stability ( $^{\circ}\text{C}$ ) was measured by CD. The value for RFX037.D was determined in the presence of 250 mM GdHCl. <sup>b</sup>Dissociation constants for L-VEGF-A (nM) were measured by surface plasmon resonance. The value for RFX001.D was reported previously.

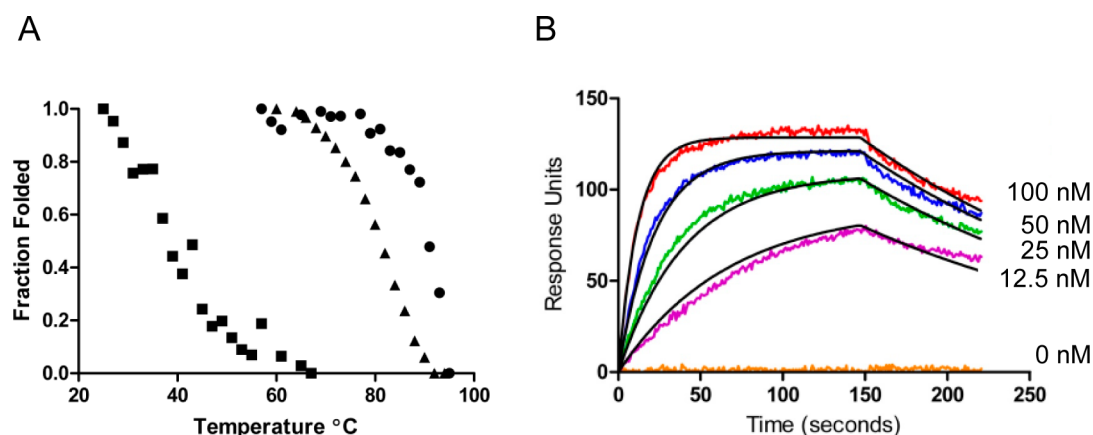


**Figure 1.** Temperature-induced denaturation and kinetic analysis. (A) Thermal denaturation of RFX001.D (squares,  $T_m = 33^{\circ}\text{C}$ ), RFX035.D (triangles,  $T_m = 82^{\circ}\text{C}$ ), and RFX037.D (circles,  $T_m = 93^{\circ}\text{C}$ ) was monitored by CD at 222 nm. The RFX037.D sample contained 250 mM GdHCl. (B) Kinetic analysis of RFX037.D binding to immobilized L-VEGF-A. The surface plasmon resonance traces are shown for RFX037.D injected at four different concentrations ranging from 12.5 to 100 nM. The curves were fit to a 1:1 Langmuir model using Prism graphpad software. A global fit yielded the following binding parameters:  $k_{\text{on}} = 7.95 \pm 0.04 \times 10^5 \text{ s}^{-1} \text{ M}^{-1}$ ,  $k_{\text{off}} = 5.11 \pm 0.05 \times 10^{-3} \text{ s}^{-1}$ ,  $K_D = 6.43 \pm 0.07 \text{ nM}$ .

are accessible by chemical synthesis and can be engineered to improve stability, affinity, and pharmacokinetics. These molecules hold great potential as alternatives to conventional recombinant protein therapeutics.<sup>6–20</sup>

As a step toward generating D-protein therapeutics, we recently developed RFX001.D, a D-protein antagonist of angiogenic vascular endothelial growth factor A (VEGF-A), using a combination of total chemical protein synthesis and mirror image phage display of proteins.<sup>21</sup> A phage library was created by designed mutagenesis of the 56-residue B1 domain of streptococcal protein G (GB1), and the library was screened against the mirror image protein D-VEGF-A.<sup>22,23</sup> The lead molecule RFX001.L had good affinity for D-VEGF-A, and conversely, its synthesized D-form enantiomer RFX001.D bound specifically to natural VEGF-A, showing reciprocal chiral specificity. The X-ray crystal structure of the heterochiral complex of RFX001.D and L-VEGF-A revealed that the D-protein antagonist bound to the region of VEGF-A that interacts with the VEGF receptor-1 (VEGFR1). Despite these promising results, RFX001.D was unsuitable for further development because it is unstable at physiological temperatures (Table 1).

Here, we describe RFX035.D and RFX037.D, D-protein variants of RFX001.D engineered for greatly improved thermal stability and affinity. RFX037.D proved to be extremely stable ( $T_m > 95^{\circ}\text{C}$ ), bound with high affinity to natural VEGF-A ( $K_d = 6 \text{ nM}$ ) and antagonized binding to VEGFR1. Elucidation of the crystal structure of RFX037.D in complex with L-VEGF-A and comparison with the previously reported structure of the RFX001.D:L-VEGF-A complex revealed that the binding interfaces involve identical residues. However, compared with RFX001.D, RFX035.D and RFX037.D have additional residues at their N- and C-termini (Table 1). In the structure of

RFX037.D, these extensions contribute to an extensive hydrogen bond network that likely confers the dramatic improvement in thermal stability.

RFX037 was further characterized for *in vivo* stability and immunogenicity. RFX037.D was metabolically stable in plasma, whereas RFX037.L was degraded rapidly. Furthermore, whether dosed subcutaneously or intravenously in mice, RFX037.D had a longer serum half-life than RFX037.L. Significantly, RFX037.D was nonimmunogenic in contrast to the strong immune response triggered by RFX037.L. These results confirm the utility of synthetic D-proteins as viable alternatives to therapeutic antibodies and L-proteins and support the continued development of RFX037.D as a therapeutic antagonist of angiogenesis.

## RESULTS AND DISCUSSION

In an effort to improve stability, two D-protein variants of RFX001 were designed to contain additional amino acid sequences at their N- and C-termini (Table 1). This strategy was based on the observation that a bacterially expressed variant of RFX001 (RFX035.L) had higher affinity for D-VEGF-A than chemically synthesized RFX001.L ( $K_d = 95 \text{ nM}$ )<sup>23</sup> and contained an N-terminal His10 tag attached to a three-residue linker plus five extra residues at its C-terminus. Thus, RFX035.D was designed as the D-enantiomer of RFX035.L. In addition, RFX037.D was designed to examine the effect of a shorter N-terminal Arg5 tag in place of the His10 tag of RFX035.D.

**Protein Synthesis.** A novel one-pot native chemical ligation and desulfurization method was devised to synthesize the full-length polypeptides RFX035.L, RFX035.D, RFX037.L, and RFX037.D. For each protein, Ala33–Ala34 of the RFX001 core peptide sequence was used as the ligation site for joining

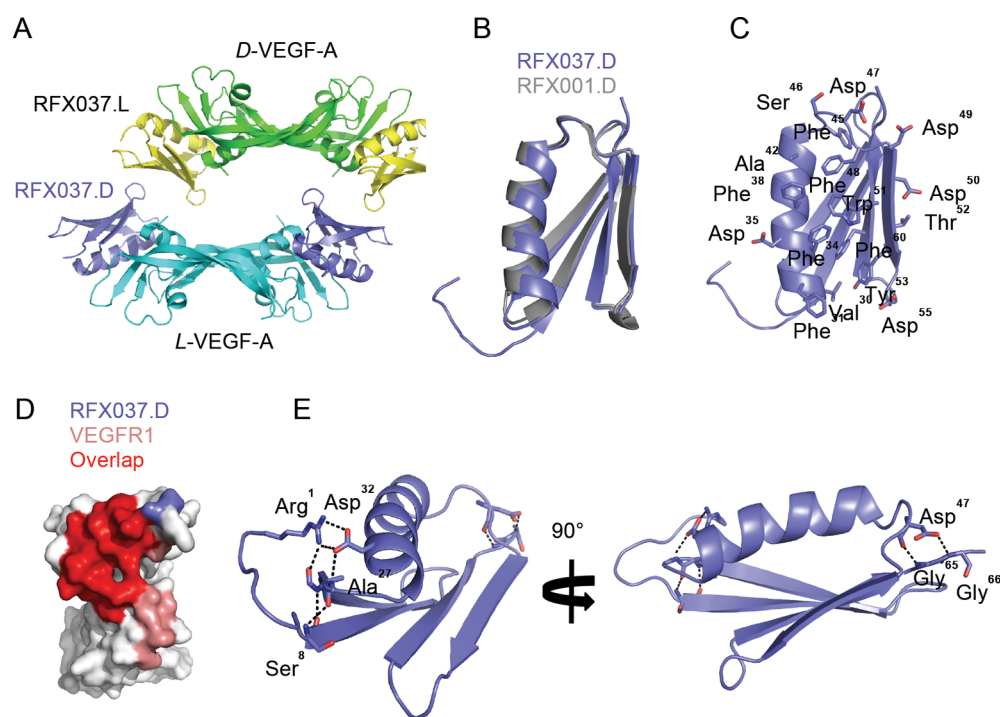


**Figure 2.** X-ray crystal structure of RFX037:VEGF-A heterochiral protein complex. (A) The asymmetric unit in space group  $P2_1$  contains two RFX037.L molecules (yellow) bound to one D-VEGF-A homodimer (green) and two RFX037.D molecules (blue) bound to one L-VEGF-A homodimer (cyan). (B) Superposition of RFX037.D (blue) and RFX001.D (gray, rcsb accession 4GLS). (C) RFX037.D side chains (shown as sticks) that contact L-VEGF-A. (D) The contact surfaces of L-VEGF-A to RFX037.D (blue), VEGFR1 (salmon), or both (red). (E) Hydrogen bond networks formed by intramolecular polar contacts originated from additional N- and C-terminal residues in RFX037.D.

the two synthetic peptide segments (bold and italic in Table 1). To support native chemical ligation, Ala34 was initially replaced by Cys34, which was subsequently desulfurized to regenerate native Ala34. The two peptide segments were synthesized using manual *in situ* neutralization Boc chemistry solid phase peptide synthesis protocols.<sup>24</sup> After assembly of the resin-bound peptide chains, the peptides were cleaved and simultaneously deprotected by treatment with anhydrous hydrogen fluoride, recovered by ether precipitation after removal of hydrogen fluoride, then purified by reverse phase high performance liquid chromatography (HPLC). Native chemical ligation of the peptide segments was carried out in phosphate buffer (pH 7.0) containing 6 M guanidium chloride (GnHCl) and 4-mercaptophenylacetic acid as the thiol catalyst.<sup>25,26</sup> After completion of ligation, the reaction mixture was treated with freshly prepared nickel boride to effect quantitative desulfurization of Cys34 to yield Ala34.<sup>26</sup> Full-length polypeptide was purified from the crude mixture by reverse phase HPLC and characterized by liquid chromatography–mass spectrometry (LC-MS; Figures S1 and S2). Full details of the chemical synthesis of RFX035.L, RFX035.D, RFX037.L, and RFX037.D are in the Supporting Information. The synthesis of RFX001.L and RFX001.D was reported previously.<sup>23</sup>

**Thermal Stability.** To determine whether the N- and C-terminal extensions improved conformational stability, thermal denaturation experiments were conducted in phosphate buffered saline (pH 7.4) and monitored by circular dichroism (CD) at 222 nm. As expected, RFX001.D was unstable at physiological temperatures with a  $T_m$  of 33 °C (Figure 1A). In contrast, thermal melting of the variants occurred at higher temperatures. RFX035.D proved to be very stable with a  $T_m$  of 82 °C (Figure 1A). Surprisingly, the loss of molar ellipticity

classically seen upon protein denaturation was not seen for RFX037.D, suggesting that this protein did not denature at 95 °C. To confirm the highly stable nature of RFX037.D, thermal denaturation was recorded in the presence of the chaotrope GnHCl. Even with the addition of 250 mM GnHCl, an extremely high  $T_m$  value of 93 °C was recorded for RFX037.D (Figure 1A).

**Binding Kinetics and Affinity.** The binding kinetics of RFX037.D for L-VEGF-A were measured by surface plasmon resonance (Figure 1B), and the affinity was calculated to be in the single-digit nanomolar range ( $K_d = 6$  nM), which was significantly tighter than the previously reported value for RFX001.D ( $K_d = 85$  nM).<sup>23</sup> RFX037.D significantly inhibited VEGF-A binding to VEGFR1 as measured by biolayer interferometry (Figure S3), an *in vitro* assay in which the extracellular domain of VEGFR1 was immobilized on a sensor tip and VEGF-A165 binding to the sensor tip was measured after exposure to different concentrations of inhibitors.

**Structural Analysis.** RFX037.D bound to L-VEGF-A with high affinity and was the most thermally stable variant, suggesting that the N-terminal Arg5 moiety may participate in stabilizing the tertiary structure or may be a component of the binding interface with L-VEGF-A. To investigate the precise role of the Arg5 moiety, we solved the crystal structure of the heterochiral VEGF-A:RFX037 complex at 2.1 Å resolution by using racemic protein crystallography (Table S1). The structure shows that two RFX037.L proteins bind to opposite poles of a D-VEGF-A homodimer and two RFX037.D proteins bind to the analogous epitopes of a L-VEGF-A homodimer (Figure 2A). Residues 9 through 64 of RFX037 superposed with the corresponding residues 1 through 56 of RFX001 with a very low C-alpha root-mean-square deviation of 0.49 Å (Figure



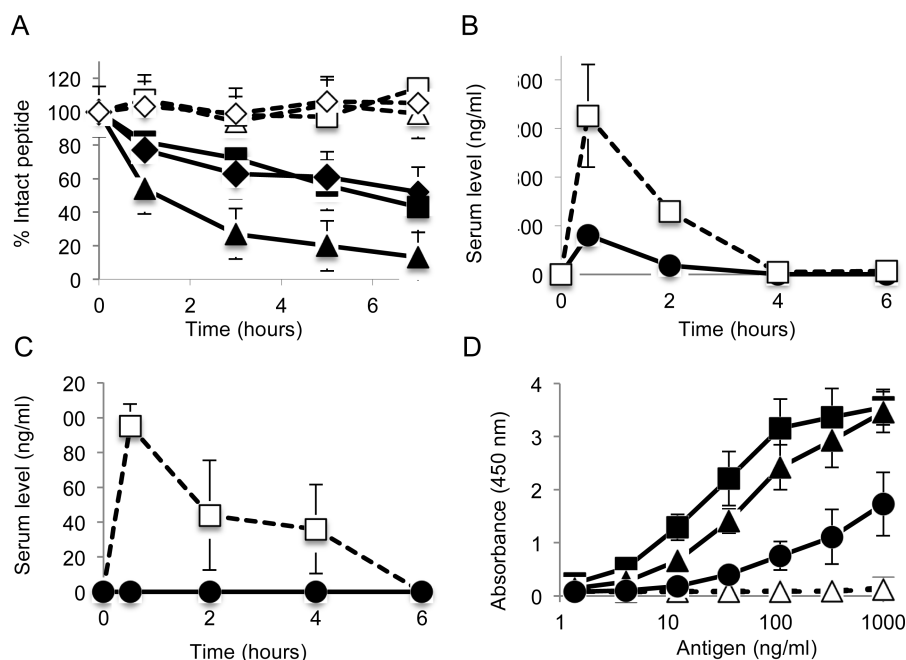


**Figure 3.** Plasma stability, pharmacokinetics, and immunogenicity of RFX037.L (solid symbols, solid lines) and RFX037.D (open symbols, dashed lines). (A) Stability in mouse (triangles), cynomolgus monkey (squares), or human (diamonds) plasma. (B) Serum levels following intravenous injection (10 mg/kg) in mice. (C) Serum levels following subcutaneous injection (10 mg/kg) in mice. (D) ELISA for measurement of serum antibody binding to antigen immobilized at varying concentrations. Sera were collected from BALB/c mice given three subcutaneous injections with 5 (circles), 20 (triangles), or 50 (squares)  $\mu\text{g}/\text{injection}$  of RFX037.L or RFX037.D emulsified in adjuvant. The mean absorbance value for five animals  $\pm$  SEM is shown. See “Methods” for further details.

2B), showing that the structures of the main chains are essentially identical in these regions. Superposition of the RFX001.D:L-VEGF-A and RFX037.D:L-VEGF-A complex structures revealed that the residues involved in binding L-VEGF-A are identical for RFX001.D and RFX037.D. In total, 17 residues on RFX037.D make contact with L-VEGF-A and contribute to a large contact surface area of 1350  $\text{\AA}^2$  at the binding interface (Figure 2C). On L-VEGF-A, the contact surfaces with RFX037.D and VEGFR1 overlap significantly (Figure 2D), consistent with the VEGFR1 antagonist activity of RFX037.D (Figure S3).

The structure also provides insights into how the N- and C-terminal extensions (Figure S4A) may contribute to the enhanced stability of RFX037.D compared with RFX001.D. Both termini of RFX037 project away from the binding interface, and thus do not interact directly with VEGF-A. The eight-residue N-terminal extensions of the two independent RFX037.D molecules in the asymmetric unit present somewhat different main chain conformations (Figure S4B), but in both cases the extension doubles back to form a salt bridge between the side chains of Arg1 and Asp32 (Figure 2E). The N-terminal salt bridge initiates an extensive hydrogen bond network that spans the width of the GB1 domain to complete an indirectly bonded cyclical peptide loop of the N-terminal extension. Specifically, Arg1 and Asp32 participate in additional hydrogen bonds with the carbonyl of Glu26 or with the amide nitrogen of Val28, respectively. These flanking hydrogen bonds position the amide and carbonyl of Ala27 to form hydrogen bonds with the amide and carbonyl of Ser8. Furthermore, the C-terminal Gly65 and Gly66 residues form hydrogen bonds that are mediated through the main chain or side chain of Asp47, respectively. These additional hydrogen bond networks likely

stabilize the protein tertiary structure to confer the high thermal stability and improved affinity of RFX037.D.

**Protease Resistance and Plasma Stability.** D-Proteins are expected to have inherent resistance to proteolytic degradation. However, in addition to D-amino acids, RFX037.D contains the achiral amino acid glycine, and therefore the resistance of RFX037.D to proteases was examined and compared with that of RFX037.L by incubating each synthetic protein with papain, a protease widely distributed in nature, and Pronase, which contains a mixture of proteases. The progress of protein degradation was monitored by HPLC (Figure S5). After 16 h, RFX037.L was nearly completely degraded, while RFX037.D remained undigested, demonstrating that RFX037.D is resistant to proteolysis. This also suggested that RFX037.D should be non- or minimally immunogenic, as protein processing is necessary to elicit a strong MHC-assisted immune response.<sup>27</sup> Additionally, D-peptides can be differentially presented by MHC class II receptors compared to L-enantiomers, which often reduces their immunogenicity.<sup>28–31</sup>

The stabilities of the L- and D-enantiomers of RFX037 in plasma were assessed by measuring the degradation of the proteins by LC-MS/MS following incubation in mouse, monkey, or human plasma (Figure 3A). RFX037.L was degraded in all three plasma types with the degradation in mouse plasma occurring more quickly than in monkey or human plasma, which were indistinguishable from each other. In contrast, RFX037.D showed no appreciable degradation in any of the plasma types.

**In Vivo Stability and Clearance.** LC-MS/MS analysis was also used to assess the *in vivo* stability and clearance of RFX037.L and RFX037.D after intravenous or subcutaneous administration in male CD-1 mice. After intravenous infusion,

RFX037.D reached an approximately 4-fold higher serum concentration than RFX037.L at the first measured time point (30 min) and was cleared from the serum after 4 h (Figure 3B). In contrast, the L-enantiomer was essentially cleared from the serum after 2 h. The disappearance of the D-protein from the serum after 4 h is consistent with a renal clearance mechanism, which was expected based on the small size of the protein. The more rapid clearance of RFX037.L was likely due primarily to proteolysis and metabolism rather than renal clearance. After subcutaneous administration, RFX037.D reached a maximum serum concentration at the first measured time point (30 min) and was cleared by 6 h (Figure 3C). In contrast, RFX037.L never reached measurable levels in the serum after subcutaneous administration.

**Immunogenicity.** Previous studies using linear and multi-chain polypeptides composed entirely of D-amino acids showed that, when injected at low doses, these polypeptides can induce an immune response.<sup>28,32,33</sup> This response could not be boosted with subsequent injections and repeated low dose injections, or exposure to high doses led to tolerance against these antigens. In general, immune responses to the D-peptide antigens was thymus-independent,<sup>34</sup> as these peptides were metabolically stable.<sup>35</sup> However, if >3% of the polymer was replaced with L-amino acids<sup>33</sup> or was conjugated to a carrier L-peptide or L-protein,<sup>30</sup> the response became thymus-dependent, possibly due to presentation of L-epitopes on MHC class II molecules. In fact, there are several reports in the literature where retro-inverso D-peptides have been used as immunogens after conjugation to a carrier L-protein or L-peptide.<sup>36–39</sup>

The objective of some of the above-described studies was to make an effective immunogen as opposed to avoiding immune response to a potential therapeutic molecule. Moreover, all of these studies involved small linear peptides that do not require processing<sup>28</sup> instead of well-folded D-proteins. Therefore, we thought it possible that folded D-proteins may be non-immunogenic, as reported by Dintzis *et al.*<sup>5</sup> Because the immune responses seen with multichain D-amino acid polymers were dose-dependent, we decided it would be prudent to study the effect of dosage on the immune response.

To assess the *in vivo* immunogenicity of the L- and D-proteins, BALB/c mice were immunized with three injections of low (5  $\mu\text{g}$ ), medium (20  $\mu\text{g}$ ), or high (50  $\mu\text{g}$ ) doses of antigen in combination with a potent adjuvant (Figure 3D). Sera were collected after 42 days, and the presence of anti-RFX037.L or anti-RFX037.D circulating antibodies was measured by ELISA. Sera from all mice immunized with RFX037.L showed strong binding to immobilized RFX037.L by ELISA, and binding activity was dependent on the coating concentration of antigen. The highest binding activity was observed in sera from mice immunized with the high dose followed by the medium and low dose sera. In contrast, sera from all mice immunized with RFX037.D showed no binding to RFX037.D at all coated antigen concentrations. RFX037.L or RFX037.D immune sera did not exhibit binding activity to the opposite enantiomeric form of the antigen (data not shown). These results are consistent with the hypothesis that proteins composed of D-amino acids and achiral glycine are non-immunogenic, even when immunized with a strong adjuvant. The absence of any immune response when the D-proteins were immunized at low, medium, or high doses contrasts with earlier unexplained results that some D-amino acid polymers were only immunogenic at low doses.<sup>29</sup>

**Conclusions.** Protein therapeutics benefit from their inherent large protein–protein interaction surfaces, maximizing specificity and affinity toward their targets while minimizing off target effects. However, the half-life of proteins can be short due to their *in vivo* proteolysis and metabolism, limiting their potency and increasing their dosing frequency. In addition, repeated dosing can often lead to immunogenicity issues, limiting their long-term use. Here, we address these issues by demonstrating dramatic differences between otherwise identical L- and D-proteins with respect to their resistance to proteolytic degradation, plasma stability, *in vivo* half-life, and immunogenicity. In contrast to the L-protein RFX037.L, the D-protein RFX037.D was completely resistant to proteolysis and metabolism in mouse, monkey, and human plasma; had a longer *in vivo* half-life when dosed by intravenous infusion or subcutaneous injection; and had a complete lack of immunogenicity, even when dosed in combination with a strong adjuvant. Moreover, RFX037.D bound to natural VEGF-A with an affinity comparable to those of antibodies and proved to be even more stable than therapeutic antibodies. Together, these observations suggest that D-proteins have inherent properties that could make them an important new class of pharmaceutical products, and our results demonstrate that stereochemistry is a fundamental property of proteins that regulates immunogenicity and metabolic stability.

## METHODS

**Chemical Protein Synthesis.** The D-proteins were prepared by total chemical synthesis. Full details are provided in the Supporting Information.

**Thermal Denaturation.** The thermal denaturation measurements of RFX001.D and RFX035.D were recorded using an AVIV-202 CD spectrophotometer (Aviv Biomedical, Lakewood, NJ, USA), while those of RFX037.D were recorded using a JASCO J-1500 spectrometer (JASCO Instruments, Easton, MD, USA). Each protein sample (0.4 mg mL<sup>-1</sup>) was monitored at 222 nm in a 0.1 cm path length CD cuvette over the temperature range 10–95 °C in increments of 2.5 °C, with 90 s equilibration time and averaging over 5 s. RFX001.D and RFX035.D were assayed in phosphate-buffered saline, pH 7.4 (PBS). RFX037.D was assayed in PBS with 250 mM GnHCl.

**Surface Plasmon Resonance.** Synthetic L-VEGF-A (0.25 mg mL<sup>-1</sup>) and D-VEGF-A (0.25 mg mL<sup>-1</sup>) were immobilized in separate flow cells of a GLM sensor chip in a ProteOn Protein Interaction Array System (Bio-Rad) using an amine coupling kit (EDC/NHS). Sensorgrams were generated by injecting several concentrations (12.5–100 nM) of protein ligand over the chip. The interactions were analyzed by global kinetic analysis using nonlinear regression fits (Langmuir model).

**Biolayer Interferometry.** Measurements were carried out using a ForteBio Octet instrument. A VEGFR1 sensor was prepared using antihuman IgG(Fc) sensors (ForteBio). The sensor tips were incubated with rhVEGFR1/hIgGFc (R&D Systems) followed by a quenching incubation with 1  $\mu\text{M}$  human IgG (Jackson ImmunoResearch). Wavelength shifts for VEGF165 binding to the VEGFR1 sensor at each inhibitor concentration were normalized by subtracting the wavelength shift of the inhibitor alone. Percent inhibition was calculated using the wavelength shift for VEGF165 binding in the absence of inhibitor as 0% and the wavelength shift for VEGF165 binding with a nonreactive sensor as 100%.

**Crystallization, Structure Determination, and Refinement.** For crystallization, the racemic protein solution was prepared by mixing 1 equiv of L-VEGF-A (2.72 mg mL<sup>-1</sup>), 1 equiv of D-VEGF-A (2.72 mg mL<sup>-1</sup>), 2 equiv of RFX037.D (0.89 mg mL<sup>-1</sup>), and 2 equiv of RFX037.L (0.89 mg mL<sup>-1</sup>) in aqueous buffer containing 10 mM HEPES, at pH 7.0. Racemic crystals of the VEGF-A:RFX037 complex were grown at 19 °C using the hanging drop vapor diffusion technique

with 1  $\mu\text{L}$  of protein solution and 1  $\mu\text{L}$  of reservoir solution placed over 1 mL of reservoir solution containing 0.1 M  $\text{MgCl}_2$ , 0.1 M HEPES (pH 7.0), and PEG3350 (11% v/v; Pro-complex suit, catalogue number 130715). Crystals appeared within 7 days. Selected crystals were flash frozen in liquid nitrogen after a brief wash in the cryoprotectant (reservoir solution plus 20% (v/v) glycerol). A complete data set to 2.1 Å was collected from a single crystal at 100 K using 0.97 Å wavelength synchrotron radiation at the Argonne National Laboratory (Advanced Photon Source, beamline 24-ID C, equipped with ADSC Q315 CCD detector).

Crystal diffraction images were indexed, integrated, scaled, and merged with HKL2000. Examination of the diffraction intensity statistics revealed that the protein complex racemate was crystallized in a centrosymmetric space group  $P21/n$ . Cell content analysis suggested that the crystal most likely contained one VEGF-A homodimer and two RFX037 molecules in the asymmetric unit. The structure was solved by molecular replacement with the program PHASER<sup>40</sup> using the previously reported X-ray structure of the RFX001.D:L-VEGF-A complex (PDB accession code 4GLN) as a search model.<sup>23</sup> The resulting protein complex model was refined with PHENIX.REFINE<sup>41</sup> using a maximum likelihood target function. After each refinement step, the model was visually inspected in COOT<sup>42</sup> using both  $2F_o - F_c$  and  $F_o - F_c$  difference maps. The final model had an Rfactor (Rfree) of 26.1% (30.7%). The structure was also solved in the lower symmetry space group P21 using the noninverted and inverted coordinates of the structure solved in  $P21/n$ . The final model refined in space group P21 had an Rfactor (Rfree) of 22.2% (28.2%). X-ray crystal diffraction data and refinement statistics of the heterochiral protein complex racemate in both the  $P21$  and  $P21/n$  space groups are listed in Table S1. Figures were rendered in PYMOL, and buried surfaces were calculated using PISA.

**Proteolysis Assays.** RFX037.L or RFX037.D (25  $\mu\text{M}$ ) was incubated with papain or Pronase (2.5  $\mu\text{M}$ ) in PBS at RT for 16 h, and the solutions were analyzed by HPLC.

**Preparation of Calibration Standards for Plasma and Serum Analysis.** Stock solutions of peptides (1 mg  $\text{mL}^{-1}$ ) were prepared in PBS and stored at 2–8 °C. Serum calibration standards were prepared by serial dilution in mouse serum. The peptide calibration concentrations were 50, 100, 250, 500, 1000, 2500, 5000 and 10 000 ng/mL.

**Preparation of Samples for *in Vitro* Plasma Stability Analysis.** Peptide stock solutions (1 mg  $\text{mL}^{-1}$ ) were used to prepare 20  $\mu\text{g}/\text{mL}$  of peptide working solutions in 10:90 (v/v) methanol/water, and these were stored in a refrigerator at 2–8 °C. Plasma stability samples were prepared by adding 225  $\mu\text{L}$  plasma into vials containing 25  $\mu\text{L}$  of 20  $\mu\text{g}/\text{mL}$  peptide working solutions at each time point (0, 1, 3, 5, and 7 h) for incubation at RT.

**Biological Sample Extraction by Solid Phase Extraction (SPE).** Plasma and serum samples were prepared using SPE to enrich the peptides and remove the endogenous components such as serum proteins, lipids, and salts. Oasis HLB  $\mu\text{Elution}$  96-well SPE plates were used and conditioned by sequential addition of 400  $\mu\text{L}$  methanol and water under a vacuum. A 25  $\mu\text{L}$  plasma or serum sample was aliquoted into the appropriate well of a 96-well plate, followed by the addition of 50  $\mu\text{L}$  of 0.1 M NaOH and, after mixing, 300  $\mu\text{L}$  of 10% MeOH. The pretreated samples were transferred to the conditioned 96-well SPE plate and drawn through with a vacuum. The plate was washed sequentially with 100  $\mu\text{L}$  of water, then 10% MeOH with 2%  $\text{NH}_4\text{OH}$ , and finally water again. The final extract was eluted into a 96-well plate with 30  $\mu\text{L}$  of methanol/water (90:10, v/v) containing 0.1% formic acid, and the eluate was diluted with 30  $\mu\text{L}$  of water. The 96-well plate was capped with a polypropylene cover and transferred to the autosampler. Samples were injected onto the LC-MS/MS system for analysis.

**Chromatography and Mass Spectrometry for Plasma and Serum Analysis.** The LC-MS/MS consisted of an Acquity UPLC system (Waters, Milford, MA) coupled to a 6500 QTRAP mass spectrometer (AB Sciex, Toronto, Canada) with a Turbo IonSpray ionization source operated in the positive ion mode. The analytical column was an Aeries C4 2.1  $\times$  100 mm (Phenomenex, Torrance,

CA). A 0.2  $\mu\text{m}$  precolumn filter unit was used to protect the analytical column. The mobile phases of 0.1% formic acid in acetonitrile/water (5:95, v/v, mobile phase A) and 0.1% formic acid in acetonitrile/water (95:5, v/v, mobile phase B) were delivered under gradient programs for 5 min. The LC gradients in minutes per percent of mobile phase B were 0.0/15, 0.5/15, 3.0/35, 3.1/95, 4.5/95, 4.6/15, and 5.0/15 for ubiquitin as control peptides and 0.0/25, 0.5/25, 3.0/35, 3.1/95, 4.5/95, 4.6/25, and 5.0/25 for RFX037.L and RFX037.D. The flow rate was 0.5 mL/min with a column temperature of 70 °C. MRM parameters were optimized by direct infusion of 10  $\mu\text{g}/\text{mL}$  of peptide tuning solutions. The ESI spray voltage was set at 5000 V. The source temperature was 500 °C. The curtain gas (CUR) was 30. The nebulizer gas setting (GS1) was 40, and the auxiliary gas setting (GS2) was 50 (all arbitrary units). The ion transitions for MS/MS detection were  $m/z$  754.0  $\rightarrow$  817.3 for ubiquitin and  $m/z$  867.9  $\rightarrow$  815.8 for RFX037.L and RFX037.D.

**Data Analysis for Plasma and Serum Analysis.** Data were collected and processed using AB Sciex Analyst software (version 1.6.2). The plasma stability of the tested peptides was derived from the peak area at each time point corresponding to peptides obtained from the LC-MS/MS analysis. All data were normalized to the value at the 0 h time point as the percentage of intact peptide and plotted against incubation time for the stability profile of each peptide. For pharmacokinetic study samples, the calibration curve was derived using  $1/x^2$  weighted linear regression of the peak area versus the concentration of the corresponding standard. The regression equation from the calibration standards was used to back-calculate the measured concentration for each standard, control, and unknown sample.

**Pharmacokinetic Studies.** Serum samples were collected from male CD-1 mice after dosing subcutaneously or by intravenous bolus administration with each peptide at 10 mg/kg according to a protocol approved by the Institutional Animal Care and Use Committee of Amgen, Inc. The samples were frozen and stored at –70 °C until LC-MS/MS analysis.

**Immunization and Immunogenicity Assays.** Five BALB/c mice per group were given three subcutaneous injections in the back of the neck on days 0, 21, and 35 with 5, 20, or 50  $\mu\text{g}/\text{injection}$  of RFX037.D or RFX037.L antigen emulsified in Alhydrogel/MurNac-L-Ala-D-isoGln (ALD/MDP) as described.<sup>43</sup> Immune sera were collected on day 42.

ELISAs were performed in EIA/RIA 96-well microtiter plates (Corning) using 50  $\mu\text{L}$  incubation volumes. Between each incubation step, wells were washed four times with 200  $\mu\text{L}$  of PBS with 0.05% Tween 20. Wells were coated overnight at 4 °C with either RFX037.D or RFX037.L in PBS. After coating, wells were emptied and blocked with PBS-Casein (Surmodics) for 1 h at ambient temperature. Serum from each mouse was diluted 1:1000 in PBS-Casein and incubated in the wells for 1.5 h. Bound antibody was detected using Goat Anti-Mouse IgG (Fc $\gamma$  fragment specific)–HRP conjugate (Jackson ImmunoResearch) and High Kinetic TMB (Moss Substrates). After the addition of stop solution (1.0 M  $\text{H}_3\text{PO}_4$ ), absorbance was measured at 450 nm.

## ■ ASSOCIATED CONTENT

### 📄 Supporting Information

The Supporting Information is available free of charge on the ACS Publications website at DOI: 10.1021/acchembio.5b01006.

Detailed methods for peptide synthesis, LCMS data for synthesized peptides, data collection and refinement statistics for crystallography, additional data on inhibition of VEGFA–VEGFR1 interaction, and the role of tags in stabilization (PDF)

### Accession Codes

Crystallography, atomic coordinates, and structure factors have been deposited in the Protein Data Bank, [www.pdb.org](http://www.pdb.org). PDB



ID codes are SHHD (racemic complex in space group P21), and SHHC (racemic complex in space group P21/n).

## AUTHOR INFORMATION

### Corresponding Authors

\*E-mail skent@uchicago.edu.

\*E-mail sachdev.sidhu@utoronto.ca.

### Present Addresses

<sup>∇</sup>Department of Pathology and Laboratory Medicine, College of Medicine, University of Saskatchewan, SK, Canada S7N5E5.

<sup>○</sup>AbbVie, Inc., North Chicago, IL 60064, United States.

### Author Contributions

◆M.U. and D.J.L. contributed equally to this work.

### Funding

This work was supported by funds from Reflexion Pharmaceuticals, Inc., and Amgen, Inc.

### Notes

The authors declare the following competing financial interest(s): This research has been carried out at the University of Chicago and the University of Toronto as part of a research program funded by the two universities under agreements with a company, Reflexion Pharmaceuticals, Inc. Both universities have minor (< 2%) equity positions in 539 Reflexion. Ault-Riché, Kent, and Sidhu are founders of Reflexion. With the exception of Dong Jun Lee, Hongan Li, Les Miranda, and Joshua Lowitz, the other authors of this paper own equity in Reflexion, and thus each of these authors declares a conflict of interest.

## ACKNOWLEDGMENTS

Vicki Mountain helped in the preparation and writing of the manuscript. Use of NE-CAT beamline 24-ID at the Advanced Photon Source is supported by award RR-15301 from the National Center for Research Resources at the National Institutes of Health. Use of the Advanced Photon Source is supported by the Department of Energy, Office of Basic Energy Sciences, under contract no. DE-AC02-06CH11357.

## REFERENCES

- (1) Sidhu, S. S. (2012) Antibodies for all: The case for genome-wide affinity reagents. *FEBS Lett.* 586, 2778–2779.
- (2) Binz, H. K., Amstutz, P., and Pluckthun, A. (2005) Engineering novel binding proteins from nonimmunoglobulin domains. *Nat. Biotechnol.* 23, 1257–1268.
- (3) Gebauer, M., and Skerra, A. (2009) Engineered protein scaffolds as next-generation antibody therapeutics. *Curr. Opin. Chem. Biol.* 13, 245–255.
- (4) Milton, R. C., Milton, S. C., and Kent, S. B. (1992) Total chemical synthesis of a D-enzyme: the enantiomers of HIV-1 protease show reciprocal chiral substrate specificity [corrected]. *Science* 256, 1445–1448.
- (5) Dintzis, H. M., Symer, D. E., Dintzis, R. Z., Zawadzke, L. E., and Berg, J. M. (1993) A comparison of the immunogenicity of a pair of enantiomeric proteins. *Proteins: Struct., Funct., Genet.* 16, 306–308.
- (6) Chang, H. N., Liu, B. Y., Qi, Y. K., Zhou, Y., Chen, Y. P., Pan, K. M., Li, W. W., Zhou, X. M., Ma, W. W., Fu, C. Y., Qi, Y. M., Liu, L., and Gao, Y. F. (2015) Blocking of the PD-1/PD-L1 Interaction by a D-Peptide Antagonist for Cancer Immunotherapy. *Angew. Chem., Int. Ed.* 54, 11760.
- (7) Eckert, D. M., Malashkevich, V. N., Hong, L. H., Carr, P. A., and Kim, P. S. (1999) Inhibiting HIV-1 entry: discovery of D-peptide inhibitors that target the gp41 coiled-coil pocket. *Cell* 99, 103–115.

(8) Elkin, C. D., Zuccola, H. J., Hogle, J. M., and Joseph-McCarthy, D. (2000) Computational design of D-peptide inhibitors of hepatitis delta antigen dimerization. *J. Comput.-Aided Mol. Des.* 14, 705–718.

(9) Funke, S. A., and Willbold, D. (2009) Mirror image phage display—a method to generate D-peptide ligands for use in diagnostic or therapeutical applications. *Mol. Biosyst.* 5, 783–786.

(10) Liu, M., Li, C., Pazgier, M., Li, C., Mao, Y., Lv, Y., Gu, B., Wei, G., Yuan, W., Zhan, C., Lu, W. Y., and Lu, W. (2010) D-peptide inhibitors of the p53-MDM2 interaction for targeted molecular therapy of malignant neoplasms. *Proc. Natl. Acad. Sci. U. S. A.* 107, 14321–14326.

(11) Sun, N., Funke, S. A., and Willbold, D. (2012) Mirror image phage display—generating stable therapeutically and diagnostically active peptides with biotechnological means. *J. Biotechnol.* 161, 121–125.

(12) van Groen, T., Wiesehan, K., Funke, S. A., Kadish, I., Nagel-Steger, L., and Willbold, D. (2008) Reduction of Alzheimer's disease amyloid plaque load in transgenic mice by D3, A D-enantiomeric peptide identified by mirror image phage display. *ChemMedChem* 3, 1848–1852.

(13) Welch, B. D., Francis, J. N., Redman, J. S., Paul, S., Weinstock, M. T., Reeves, J. D., Lie, Y. S., Whitby, F. G., Eckert, D. M., Hill, C. P., Root, M. J., and Kay, M. S. (2010) Design of a potent D-peptide HIV-1 entry inhibitor with a strong barrier to resistance. *J. Virol* 84, 11235–11244.

(14) Welch, B. D., VanDemark, A. P., Heroux, A., Hill, C. P., and Kay, M. S. (2007) Potent D-peptide inhibitors of HIV-1 entry. *Proc. Natl. Acad. Sci. U. S. A.* 104, 16828–16833.

(15) Wiesehan, K., Buder, K., Linke, R. P., Patt, S., Stoldt, M., Unger, E., Schmitt, B., Bucci, E., and Willbold, D. (2003) Selection of D-amino-acid peptides that bind to Alzheimer's disease amyloid peptide abeta1–42 by mirror image phage display. *ChemBioChem* 4, 748–753.

(16) Wiesehan, K., and Willbold, D. (2003) Mirror-image phage display: aiming at the mirror. *ChemBioChem* 4, 811–815.

(17) Zhao, L., and Lu, W. (2014) Mirror image proteins. *Curr. Opin. Chem. Biol.* 22, 56–61.

(18) Aileen Funke, S., van Groen, T., Kadish, I., Bartnik, D., Nagel-Steger, L., Brener, O., Sehl, T., Batra-Safferling, R., Moriscot, C., Schoehn, G., Horn, A. H., Muller-Schiffmann, A., Korh, C., Sticht, H., and Willbold, D. (2010) Oral treatment with the D-enantiomeric peptide D3 improves the pathology and behavior of Alzheimer's Disease transgenic mice. *ACS Chem. Neurosci.* 1, 639–648.

(19) van Groen, T., Kadish, I., Funke, A., Bartnik, D., and Willbold, D. (2012) Treatment with Abeta42 binding D-amino acid peptides reduce amyloid deposition and inflammation in APP/PS1 double transgenic mice. *Adv. Protein Chem. Struct. Biol.* 88, 133–152.

(20) Zhan, C., Zhao, L., Wei, X., Wu, X., Chen, X., Yuan, W., Lu, W. Y., Pazgier, M., and Lu, W. (2012) An ultrahigh affinity D-peptide antagonist Of MDM2. *J. Med. Chem.* 55, 6237–6241.

(21) Schumacher, T. N., Mayr, L. M., Minor, D. L., Jr., Milhollen, M. A., Burgess, M. W., and Kim, P. S. (1996) Identification of D-peptide ligands through mirror-image phage display. *Science* 271, 1854–1857.

(22) Mandal, K., and Kent, S. B. (2011) Total chemical synthesis of biologically active vascular endothelial growth factor. *Angew. Chem., Int. Ed.* 50, 8029–8033.

(23) Mandal, K., Uppalapati, M., Ault-Riche, D., Kenney, J., Lowitz, J., Sidhu, S. S., and Kent, S. B. (2012) Chemical synthesis and X-ray structure of a heterochiral {D-protein antagonist plus vascular endothelial growth factor} protein complex by racemic crystallography. *Proc. Natl. Acad. Sci. U. S. A.* 109, 14779–14784.

(24) Schnolzer, M., Alewood, P., Jones, A., Alewood, D., and Kent, S. B. (1992) In situ neutralization in Boc-chemistry solid phase peptide synthesis. Rapid, high yield assembly of difficult sequences. *Int. J. Pept. Protein Res.* 40, 180–193.

(25) Dawson, P. E., Muir, T. W., Clark-Lewis, I., and Kent, S. B. (1994) Synthesis of proteins by native chemical ligation. *Science* 266, 776–779.

- (26) Johnson, E. C., and Kent, S. B. (2006) Insights into the mechanism and catalysis of the native chemical ligation reaction. *J. Am. Chem. Soc.* 128, 6640–6646.
- (27) Neefjes, J., and Ovaa, H. (2013) A peptide's perspective on antigen presentation to the immune system. *Nat. Chem. Biol.* 9, 769–775.
- (28) Benkirane, N., Friede, M., Guichard, G., Briand, J. P., Van Regenmortel, M. H., and Muller, S. (1993) Antigenicity and immunogenicity of modified synthetic peptides containing D-amino acid residues. Antibodies to a D-enantiomer do recognize the parent L-hexapeptide and reciprocally. *J. Biol. Chem.* 268, 26279–26285.
- (29) Herve, M., Maillere, B., Mourier, G., Texier, C., Leroy, S., and Menez, A. (1997) On the immunogenic properties of retro-inverso peptides. Total retro-inversion of T-cell epitopes causes a loss of binding to MHC II molecules. *Mol. Immunol.* 34, 157–163.
- (30) Sela, M., and Zisman, E. (1997) Different roles of D-amino acids in immune phenomena. *FASEB J.* 11, 449–456.
- (31) Nair, D. T., Kaur, K. J., Singh, K., Mukherjee, P., Rajagopal, D., George, A., Bal, V., Rath, S., Rao, K. V., and Salunke, D. M. (2003) Mimicry of native peptide antigens by the corresponding retro-inverso analogs is dependent on their intrinsic structure and interaction propensities. *J. Immunol.* 170, 1362–1373.
- (32) Janeway, C. A., Jr., and Sela, M. (1967) Synthetic antigens composed exclusively of L- or D-amino acids. I. Effect of optical configuration on the immunogenicity of synthetic polypeptides in mice. *Immunology* 13, 29–38.
- (33) Gill, T. J., 3rd, Kunz, H. W., and Papermaster, D. S. (1967) Studies on synthetic polypeptide antigens. 18. The role of composition, charge, and optical isomerism in the immunogenicity of synthetic polypeptides. *J. Biol. Chem.* 242, 3308–3318.
- (34) Sela, M., Mozes, E., and Shearer, G. M. (1972) Thymus-independence of slowly metabolized immunogens. *Proc. Natl. Acad. Sci. U. S. A.* 69, 2696–2700.
- (35) Van Regenmortel, M. H., and Muller, S. (1998) D-peptides as immunogens and diagnostic reagents. *Curr. Opin. Biotechnol.* 9, 377–382.
- (36) Briand, J. P., Benkirane, N., Guichard, G., Newman, J. F., Van Regenmortel, M. H., Brown, F., and Muller, S. (1997) A retro-inverso peptide corresponding to the GH loop of foot-and-mouth disease virus elicits high levels of long-lasting protective neutralizing antibodies. *Proc. Natl. Acad. Sci. U. S. A.* 94, 12545–12550.
- (37) Fischer, P., Comis, A., Tyler, M., and Howden, M. (2007) Oral and parenteral immunization with synthetic retro-inverso peptides induce antibodies that cross-react with native peptides and parent antigens. *Indian J. Biochem Biophys* 44, 140–144.
- (38) Fromme, B., Eftekhari, P., Van Regenmortel, M., Hoebeke, J., Katz, A., and Millar, R. (2003) A novel retro-inverso gonadotropin-releasing hormone (GnRH) immunogen elicits antibodies that neutralize the activity of native GnRH. *Endocrinology* 144, 3262–3269.
- (39) Ben-Yedidia, T., Beignon, A. S., Partidos, C. D., Muller, S., and Arnon, R. (2002) A retro-inverso peptide analogue of influenza virus hemagglutinin B-cell epitope 91–108 induces a strong mucosal and systemic immune response and confers protection in mice after intranasal immunization. *Mol. Immunol.* 39, 323–331.
- (40) McCoy, A. J., Grosse-Kunstleve, R. W., Adams, P. D., Winn, M. D., Storoni, L. C., and Read, R. J. (2007) Phaser crystallographic software. *J. Appl. Crystallogr.* 40, 658–674.
- (41) Adams, P. D., Afonine, P. V., Bunkoczi, G., Chen, V. B., Davis, I. W., Echols, N., Headd, J. J., Hung, L. W., Kapral, G. J., Grosse-Kunstleve, R. W., McCoy, A. J., Moriarty, N. W., Oeffner, R., Read, R. J., Richardson, D. C., Richardson, J. S., Terwilliger, T. C., and Zwart, P. H. (2010) PHENIX: a comprehensive Python-based system for macromolecular structure solution. *Acta Crystallogr., Sect. D: Biol. Crystallogr.* 66, 213–221.
- (42) Emsley, P., and Cowtan, K. (2004) Coot: model-building tools for molecular graphics. *Acta Crystallogr., Sect. D: Biol. Crystallogr.* 60, 2126–2132.
- (43) Kenney, J. S., Hughes, B. W., Masada, M. P., and Allison, A. C. (1989) Influence of adjuvants on the quantity, affinity, isotype and epitope specificity of murine antibodies. *J. Immunol. Methods* 121, 157–166.